Elastic *a*-Silicon Nanoparticle Backboned Graphene Hybrid as a Self-Compacting Anode for High-Rate Lithium Ion Batteries

Minseong Ko, Sujong Chae, Sookyung Jeong, Pilgun Oh, and Jaephil Cho*

Department of Energy Engineering, School of Energy and Chemical Engineering, Ulsan National Institute of Science and Technology (UNIST), Ulsan, 689-798, South Korea

ABSTRACT Although various Si-based graphene nanocomposites provide enhanced electrochemical performance, these candidates still yield low initial coloumbic efficiency, electrical disconnection, and fracture due to huge volume changes after extended cycles lead to severe capacity fading and increase in internal impedance. Therefore, an innovative structure to solve these problems is needed. In this study, an amorphous (*a*) silicon nanoparticle backboned graphene nanocomposite (*a*-SBG) for high-power lithium ion battery anodes was prepared. The *a*-SBG provides ideal electrode structures—a uniform distribution of amorphous silicon nanoparticle islands (particle size <10 nm) on both sides of graphene sheets—which address the improved kinetics and cycling stability issues of the silicon anodes. *a*-Si in the composite shows elastic behavior during lithium alloying and dealloying: the pristine particle size is restored after cycling, and the electrode thickness decreases during the cycles as a result of self-compacting. This noble architecture facilitates superior electrochemical performance in Li ion cells, with a specific energy of 468 W h kg^{-1} and 288 W h kg^{-1} under a specific power of 7 kW kg^{-1} and 11 kW kg^{-1}, respectively.

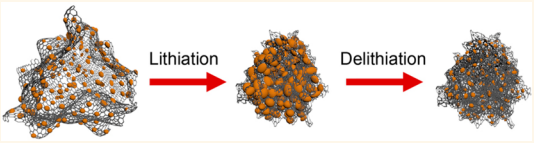

KEYWORDS: silicon anode · volume expansion · rate capability · hybrid composite · Li ion battery

The exploitation of advanced Li-ion batteries (LIB) for energy storage for many types of electronic devices requiring lightweight, long life, high power, and high energy density is a great challenge.[1−4] To meet the growing demand, alloying reaction anodes have been studied as promising alternatives to the conventional graphite anode, which has a relatively low specific capacity (372 mA h g^{-1}). However, even though Li-alloying materials (Si, Ge, Sn, Sb, *etc.*) exhibit high gravimetric and volumetric capacities, they undergo huge volume changes upon repeated Li alloying and dealloying, which create critical challenges in the electrode design and electrode materials engineering to minimize the intense mechanical degradation problems.[5−7] Recently, silicon has received a remarkable amount of attention as an alloying material because of its abundance in nature, low working potential, and exceptionally high specific capacity of 3579 mA h g^{-1} for $Li_{15}Si_4$ at room temperature.[8,9] However, because of its low intrinsic electrical conductivity (1.56×10^{-3} S m^{-1}) and extreme volume changes (>300%) during cycling,[10,11] Si suffers from limited rate capability and cycling stability due to pulverization, electrical isolation, and unstable formation of the solid-electrolyte interphase (SEI).[12−14]

To overcome these drawbacks, the engineering of various electrode materials such as nanostructures[15] (e.g., nanoparticles,[16,17] nanowires,[18,19] nanotubes,[20−22] nanoporous structures,[23,24] and their composites with carbon materials[25,26]) and other electrode design concepts (e.g., three-dimensional current collectors,[27,28] new high-performance binders,[29−32] or the binder-free concept[19]) have been suggested.

However, even though such strategies can facilitate the strain relaxation and electron transport with suppressing the mechanical fracture using their free space availability and conductive buffer effectiveness, it is still far from battery applications because of its low initial coloumbic efficiency and electrode fracture by repeated volume variation. As shown in Scheme 1a,b, electrodes composed of conventional

* Address correspondence to jpcho@unist.ac.kr.

Received for review June 17, 2014 and accepted July 31, 2014.

Published online July 31, 2014
10.1021/nn503294z

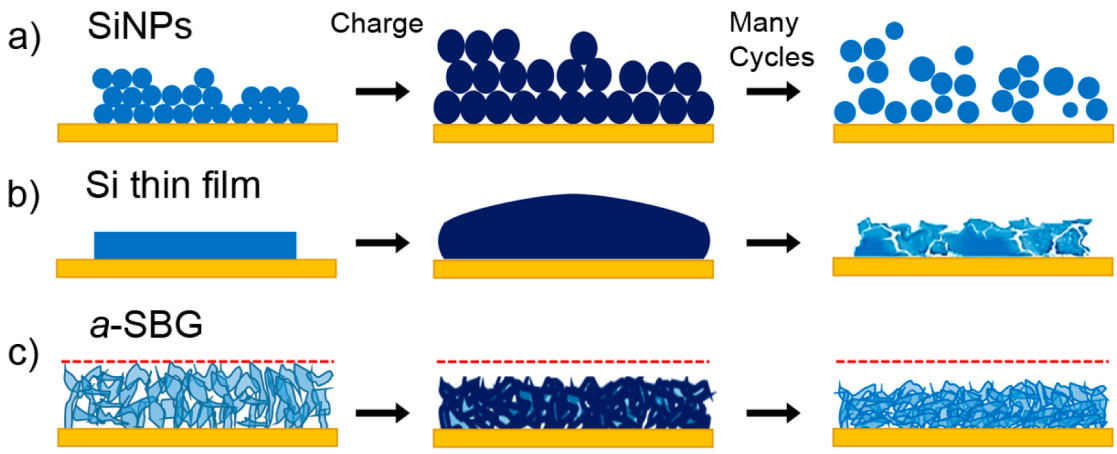

Scheme 1. Morphological and volumetric changes during electrochemical cycling in the electrode of (a) silicon nanoparticles, (b) Si thin film, and (c) *a*-SBG, which includes much free space, self-compacts during cycling, and therefore can form a stable electrode.

crystalline Si nanopowder (*c*-SiNP) or films expand upon charging and then contract during discharging, and repeated cycles eventually lead to typical electrode failure *via* drastic electrical disconnection and cracking.[14,19,33,34] However, recent a few works on patterned silicon films with amorphous phases probed the purely reversible elastic reaction with Li ions, and it was found that these films exhibited sufficient stress relief and no interconnected cracks.[35−37] In addition, the amorphous phase can offer better capacity retention and cycle life than its crystalline counterpart while providing a high Li ion diffusivity due to the presence of defects like grain boundaries and the absence of long-range order, which leads to a homogeneous lithium distribution upon lithiation.[11,38,39] Moreover, critical particle size of Si anodes is also crucial for enhancing the electrochemical performance.[16,17] Therefore, taking advantage of these characteristics of the amorphous phase and size effect to accommodate the volume change of the expanded Si host materials in an actual electrode is the most important factor for anode applications.

Among the composites with carbon material, graphene is useful in the design of high-performanace anode materials *via* simple mixing,[40,41] electrostatic assembly methods,[42,43] or chemical vapor deposition (CVD)[44,45] for LIBs due to its exceptional electronic and mechanical properties coupled with flexibility and chemical stability.[46] Hence, graphene, as an ideal matrix, plays important roles in electrodes by providing a conductive channel for electron transport and electrical contact with the electrode components and by acting as a buffer to volume changes during cycling. Nevertheless, most early studies have still had many difficulties in achieving adequate utilization of the graphene because of problems achieving homogeneous distribution of the host materials within the graphene layers and the necessity of sophisticated fabrication techniques.[47,48]

Herein, we discuss the facile method for realizing the island structure of amorphous silicon nanoparticles (*a*-SiNPs) in sizes of 5−10 nm that arranged on the electrically conductive graphene surface, namely, amorphous silicon nanoparticles backboned-graphene nanocomposite (*a*-SBG) anode, in which the *a*-SiNPs exhibit elastic behavior with strain relaxation and high Li ion diffusivity.[35−37] Furthermore, an electrode composed of the *a*-SBG nanocomposites provides unprecedented self-compacting behavior, allowing stable electrode deformation, as shown in Scheme 1c. Therefore, this hybrid architecture provides several additional benefits, as follows: (1) improvement of the Si mass loading in the composite, (2) accommodation of the volume changes without loss of SiNPs from the graphene matrix, (3) high electrical conductivity of the overall electrode, and (4) a high surface reaction area between the active materials and the electrolyte due to nanometric-size effects.

RESULTS

We first successfully fabricated the proposed *a*-SBG nanocomposites. During the fabrication process, the nonaggregated 3D porous graphene prepared by freeze-drying plays the important role of ensuring a facile pathway for SiH_4 gas penetration (see the Supporting Information, Figure S1, and Materials and Methods). With the high surface-area-to-volume ratio of porous graphene sheets, this unique SiH_4 decomposition method provides high mass loadings of Si contents up to 82 wt % as well as a uniform distribution of nanoparticles on both sides of individual graphene sheets. This in turn provides a significant enhancement of the energy density of the composite. In addition, the formation of *a*-SiNP islands prevents interference between adjacent particles during volume expansion and provides good electron transport pathways to the electrode.

Figure 1a shows the specific composition of the *a*-SBG and the behavior of its hierarchical structure in

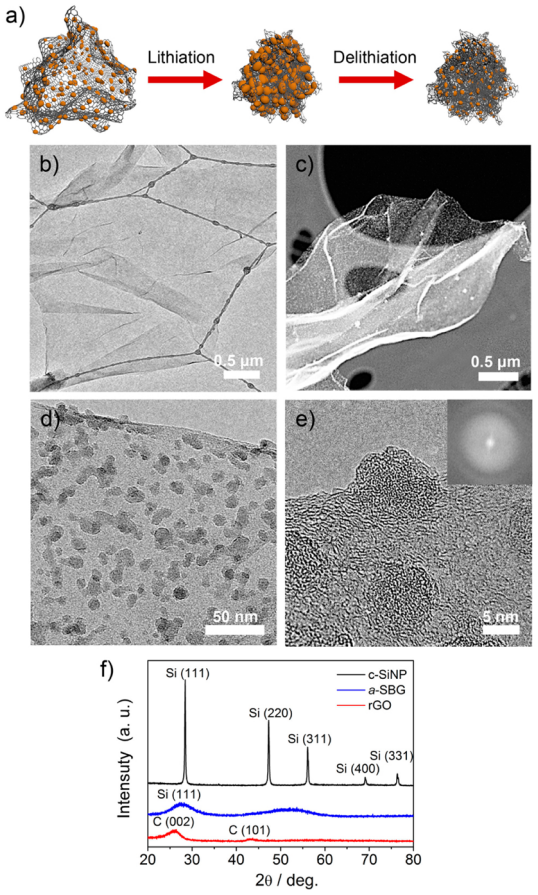

Figure 1. (a) Schematic view of *a*-SBG nanocomposites before and after electrochemical cycling. Low magnification TEM image of (b) reduced graphene oxide and (c) *a*-SBG. Higher magnification TEM images of (d) a small area of the *a*-SBG surface and (e) an individual hemispherical amorphous silicon particle, with the corresponding indexed FFT inset image. (g) Powder X-ray diffraction patterns of rGO, *a*-SBG, and *c*-SiNP.

the electrode. Graphene sheets with high defect concentrations allow facile infiltration of Li ions and provide superior interconnectivity, good structural integrity, and high electrical conductivity during cycling.[49] Furthermore, because of their flexibility, these two-dimensional (2D) curved graphene layers not only provide enough void spaces to accommodate large volume variations but also facilitate electrolyte contact (Figure 1b). In addition, the *a*-SiNPs can easily release the induced strain, and because of their short diffusion pathways and amorphous characteristics, they allow fast diffusivity and high reactivity by providing easy Li ion transport throughout the whole nanocomposite electrode. To verify its morphological, structural, and compositional features, the *a*-SBG structure was characterized using various analytical tools. The TEM image of the *a*-SBG (Figure 1c) clearly shows that the SiNPs, which appear as white dots, are extremely well distributed over the entire ultralight and transparent graphene surface. The high-magnification images (Figure 1d,e) reveal the distribution of SiNPs into islands with acceptable amounts of free space between adjacent particles, and the Fast Fourier transform (FFT) image, which is shown in the inset, confirms its amorphous structures. In addition, the Si particles of 5−10 nm in size deposited by CVD retained plane contact with the graphene surface, as shown by the large, broad peak at 28.4° (Figure 1f; see the other details in the Supporting Information, Figure S3).

Intrigued by the structural features of the *a*-SBG, we evaluated their electrochemical properties and compared them with those of crystalline silicon nanopowder (*c*-SiNP) between 0.01 and 1.5 V using coin-type lithium half-cells (2032R) at 24 °C. The rate capability tests were focused on the charge (lithium removal) rate capability rather than discharge rate capability because the charge kinetics of Si anodes are known to be slower than the discharge kinetics.[50] The first reversible lithium charge capacity of *a*-SBG is estimated to be 2858 mA h g^{-1} at a low current density of 56 mAg^{-1}, with a striking high Coulombic efficiency of 92.5% (Figure 2a). Such a high efficiency is expected to minimize the cathode capacity in a balanced Li ion cell. All the specific capacity values were estimated from the total mass of *a*-SBG, which consists of 82 wt % of silicon and 18 wt % of graphene. For comparison, a *c*-SiNP electrode was also prepared by mixing with conductive carbon black in the same weight ratio as in the *a*-SBG electrode (82:18). However, the *c*-SiNP electrode exhibited serious agglomeration and relatively loose contact between the carbon black and *c*-SiNPs,[51] and a much lower capacity of 1995 mA h g^{-1} is delivered with a relatively low Coulombic efficiency of about 75% in the first cycle. The good incorporation of the nanosized *a*-SiNP into the electrically conductive graphene is believed to allow more Li ions to be stored in the *a*-SBG than in the *c*-SiNP electrode. More exciting results were obtained for the electrode kinetics of the *a*-SBG and *c*-SiNP electrodes when their charge current densities were increased from 0.56 to 28 A g^{-1} (= 10 C) and from 0.4 to 20 A g^{-1}, respectively. For current densities of 0.56, 2.8, 14, and 28 A g^{-1}, the charge capacities of the *a*-SBG electrode were 2699, 2450, 1622, and 1148 mA h g^{-1}, respectively. On the other hand, *c*-SiNP exhibits charge capacities of 1812, 1184, 632, and 5 mA h g^{-1} when the current densities were increased from 0.56 to 2.8 to 14 to 28 A g^{-1} (Figure 2b). It is obvious that the rate capability of *a*-SBG is significantly higher than that of *c*-SiNP. Note also that the charge capacity of natural graphite rapidly decreases from 343 to 16 mA h g^{-1} with increasing current from 67 mA g^{-1} to 3 A g^{-1} (Supporting Information, Figure S4). When the current is again reduced to that used in the first cycle after 35 cycles, the specific capacity of *a*-SBG returned to the initial value, implying that the volume change of *a*-SiNP is quite reversible without pulverization. The voltage profiles obtained at different rates did not show the two-phase region below

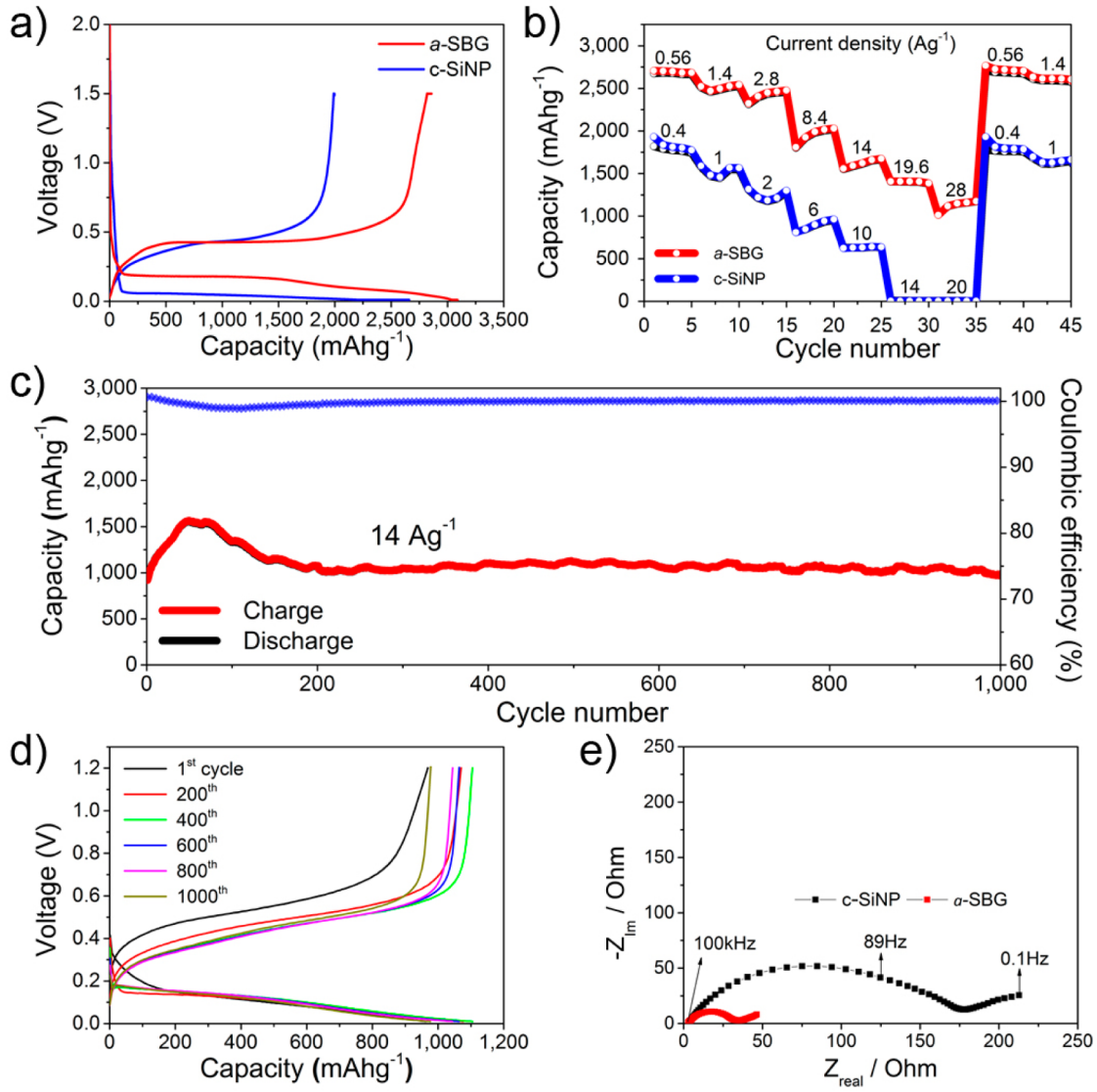

Figure 2. (a) Galvanostatic charge/discharge profiles obtained under constant current at 140 mA g^{-1} with constant voltage applied to 56 mA g^{-1} in *a*-SBG and constant current at 100 mA g^{-1} with constant voltage applied to 40 mA g^{-1} in *c*-SiNP, respectively, at the end of process in the potential range of 1.5−0.01 V. (b) Capacities of *a*-SBG and *c*-SiNP at various charge current densities from 0.56 to 28 A g^{-1} and from 0.4 to 20 A g^{-1}, respectively, with fixed discharge current densities of 0.56 and 0.4 A g^{-1}. A constant voltage of 0.01 V was applied with discharge current of 140 mA g^{-1} and 100 mA g^{-1} at the end of process. (c) Cycling performance of *a*-SBG at a charge current density of 14 A g^{-1} and a discharge density of 2.8 A g^{-1} over 1000 cycles. (d) Voltage profiles of *a*-SBG for the 1st, 200th, 400th, 600th, 800th, and 1000th cycles. (e) Nyquist plot of silicon nanoparticles and α-SBG after full lithiation at the first cycle and the equivalent circuit used to fit the impedance data.

0.1 V during the lithiation process, which is typical behavior of amorphous silicon (Supporting Information, Figure S5).[8]

Furthermore, a fast charge cycle test was carried out at a charge current density of 14 A g^{-1} for 1000 cycles, with a fixed discharge current density of 2.8 A g^{-1} (Figure 2c). Surprisingly, *a*-SBG exhibits an excellent average charge capacity of 1103 mA h g^{-1} over 1000 cycles, showing no capacity fading. The average columbic efficiency is 99.9% over all cycles. The capacity rise over the early cycles have been reported to be related with that combining the cycling kinetics improvement from electrochemical activation and side reaction from electrolyte. Indeed, similar phenomena have been observed in many previous studies of Si-based anodes.[44,52,53] In the case of fast discharge tests (Supporting Information, Figure S6), the capacities of the *a*-SBG electrode exhibited 2843, 2555, 2431, 2377, 2315 mA h g^{-1} at current of 0.56, 14, 28, 42, and 56 A g^{-1}, respectively. This excellent performance could be ascribed to the synergistic effect of the *a*-SNPs and interconnected conductive graphene layers. These results are also in good agreement with the cyclic voltammetry (CV) and electrochemical impedance spectroscopy (EIS) results. The *a*-SBG electrode delivers a higher discharge plateau and a lower charge plateau than *c*-SiNP at various scan rates from 0.4 to 1.0 mV s^{-1}, indicating smaller polarization and thus a ~4 times higher

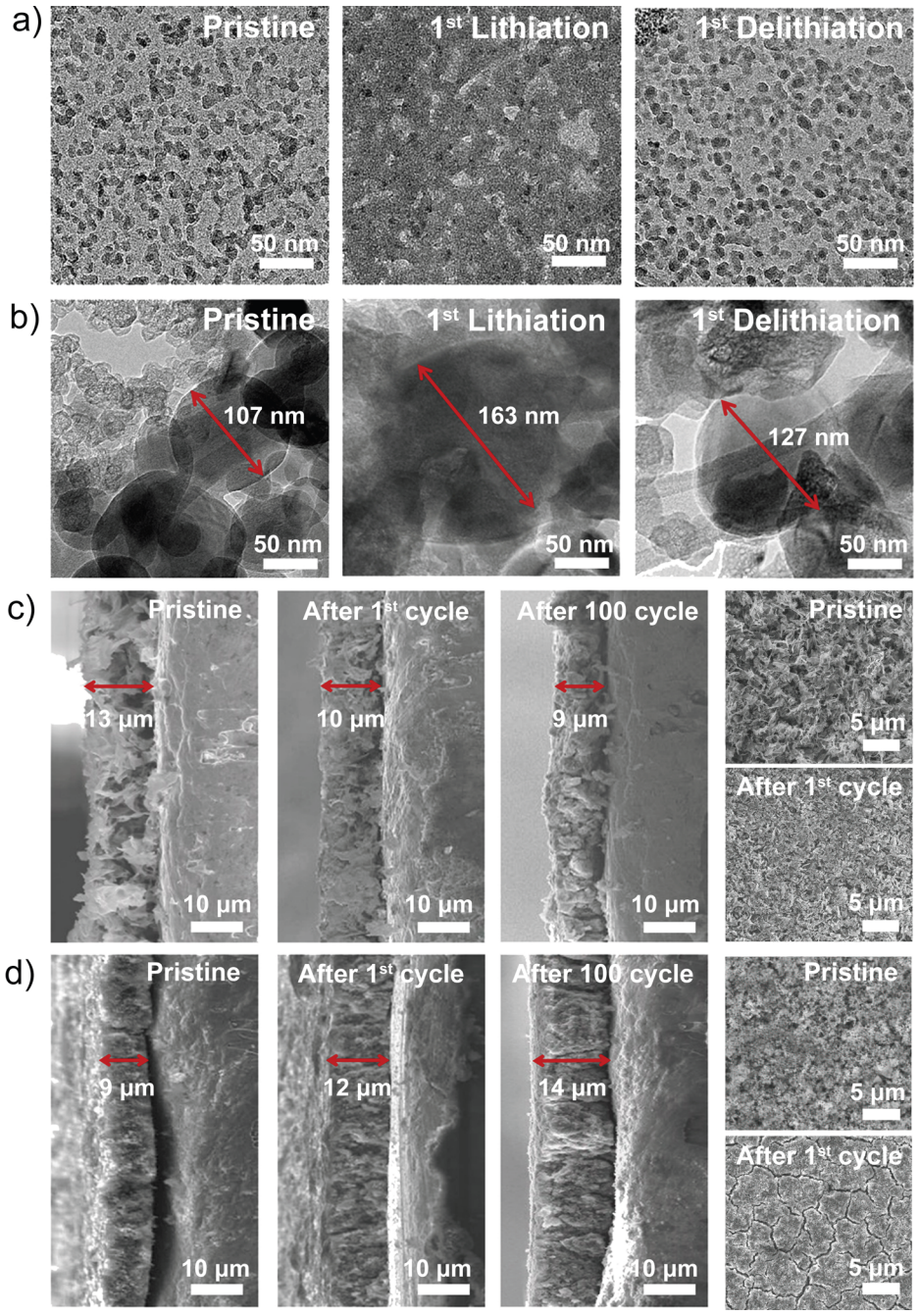

Figure 3. HR-TEM images of (a) *a*-SBG and (b) *c*-SiNPs in pristine condition, after lithiation, and after delithiation. Cross-section and top-view SEM images of (c) the *a*-SBG electrode and (d) SiNP electrode taken during electrochemical cycling. Both electrodes were fabricated with the same cell capacity. All the SEM images were taken from the same points of the electrodes.

diffusion coefficient (Supporting Information, Figure S7). Furthermore, the Nyquist plot of the *c*-SiNP electrode after lithiation to 0.01 V (Figure 2d) contains a clear semicircle with a large diameter at high frequencies, indicating development of a large charge-transfer resistance on the electrode interface. However, the *a*-SBG sample exhibits a depressed semicircle with a reduced diameter at high frequencies, suggesting significantly decreased charge-transfer resistance, which is consistent with the greatly improved performance in electrochemical behavior.

In order to observe the volume variations of single *a*-SBG and *c*-SiNP electrodes before and after full (de)lithiation, the morphological changes were investigated by SEM and HRTEM. Figure 3a clearly reveals that upon delithiation, the silicon particles convert back to their original size of 10 nm from the expanded size reached upon lithiation. Thus, the volume expansion is clearly accommodated, and the strain can be relieved without cracking. However, *c*-SiNPs of ~100 nm in size exhibited increased diameters after delithiation due to the development of residual stress originating

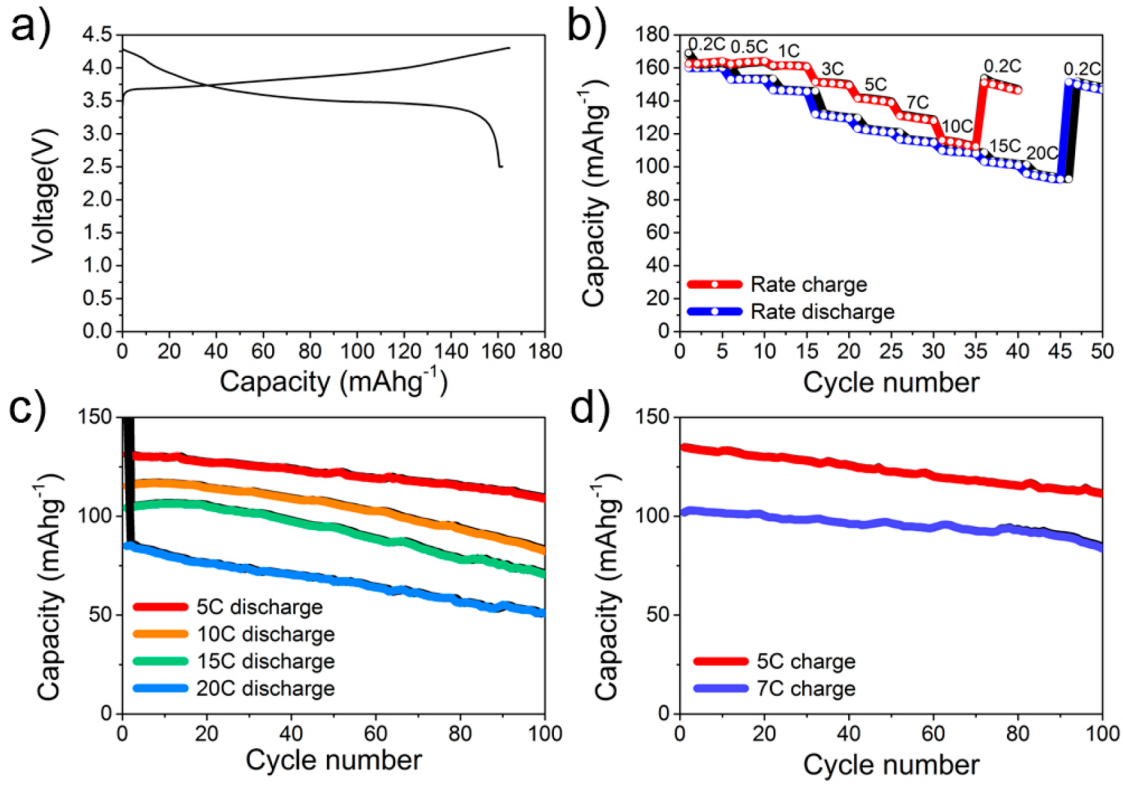

Figure 4. (a) Galvanostatic charge/discharge profile obtained under constant current a rate of 0.1 C with constant voltage applied to 0.05 C at the end of process in the potential range of 2.5−4.3 V. (b) Capacity at various charge and discharge rates from 0.2 to 10 C and from 0.2 to 20 C. The discharge and charge rates were fixed at 0.2 C, but a constant voltage of 4.3 V was applied with 0.1 C at the end of the process. (c) Cycling performance during fast discharging at rates from 5 to 20 C and (d) fast charging at rates of 5 and 7C for 100 cycles.

from plastic strain during Li insertion (Figure 3b).[54] As a consequence, repeated lithium reactions over dozens of cycles lead to catastrophic particle pulverization and electrode expansion. It has been reported that the critical size of the *c*-SNPs necessary to avoid particle pulverization is <5 nm.[16]

More interestingly, the electrode thickness changes of these two samples were examined at the same position (Figure 3c). The electrode composed of *a*-SBG surprisingly exhibits a 31% decrease in thickness from 13 to 9 μm after 100 cycles. This indicates that the loosely interconnected graphene sheets self-compacted during the cycling. As demonstrated above (Figure 1a), upon Si volume expansion, the flexible graphene can shrink to form a more stable electrode arrangement. This phenomenon has not been reported elsewhere. To accommodate the thickness change of the anode, it is a great advantage to have more spaces available in the matrix. However, the thickness of the *c*-SiNP electrode (Figure 3d) expands by 55% after 100 cycles, and severe cracks appear on its surface after only the first cycle.

Finally, a Li ion cell consisting of the *a*-SBG anode and a $LiCoO_2$ cathode was fabricated and cycled at various rates. As shown in Figure 4a, a high reversible capacity of 162 mA h g^{-1} was recorded in the first cycle in the potential range between 2.5 and 4.3 V at 24 °C. The charge (red) and discharge (blue) specific capacities measured at various rates stepwise increased from 0.2 to 10 C and to 20 C were considerably high, in the ranges of 164−112 mA h g^{-1} and 160−93 mA h g^{-1}, respectively (Figure 4b). These values correspond to specific energies of 468 and 288 W h kg^{-1} at charge and discharge rates of 10 C (= 7.0 kW kg^{-1}) and 20 C (= 11 kW kg^{-1}), respectively. Figure 4c shows the stability of the *a*-SBG electrodes over 100 cycles at ultrafast discharge rates of 5, 10, 15, and 20 C. Remarkable capacity retentions of 83, 71, 68, and 60% were obtained after 100 cycles, respectively. In addition, the full cell retains 83% and 82% of its initial capacity after 100 cycles at ultrafast charge rates of 5 and 7 C, respectively, indicating good rate capability of the *a*-SBG/LiCoO2 full cell (Figure 4d). The voltage profiles for 7 C rate charge (Figure 4d) and 20 C rate discharge (Figure 4c) cycling were plotted in Supporting Inforation, Figure S8.

CONCLUSIONS

With the sophisticated fabrication of amorphous (*a*) silicon nanoparticles backboned-graphene nanocomposite (*a*-SBG), we have successfully addressed the improved kinetics and cycling stability issues of silicon anodes. In particular, with the amorphous characteristic of island nanosilicon (particle size <10 nm) and partially

exposed graphene surface, these exquisite hybrid materials can not only have elastic behavior on volume changes and decrease in electrode thickness as a result of self-compacting but also facilitate the electron transport and lithium diffusion. As a result, remarkable first-cycle coloumbic efficiency of 92.5% with a high specific reversible capacity of 2858 mAh/g, excellent power capability, and good cycling stability were obtained. As a consequence, this successful hybrid anode design could be extended to other material systems that undergo large volume expansions with low electronic conductivity as a major breakthrough in high energy battery systems for electric vehicle or grid energy storage applications.

MATERIALS AND METHODS

Preparation of the Porous Graphene Silicon Nanocomposite. A modified Hummers method[55] was used for preparation of graphene oxide (GO) from natural graphite flake. This graphene oxide was diluted to a concentration of 0.7 mg mL^{-1} and exfoliated by sonication for 1 h. As-prepared graphene oxide (GO) solution was frozen by liquid nitrogen and freeze-dried for a few days. The freeze-dried porous graphene oxide was reduced by thermal treatment at 1000 °C for 1 h in a hydrogen atmosphere. Then, the amorphous pure silicon was deposited on each surface of the reduced graphene oxide by decomposition of SiH_4 gas at 550 °C for 30 min.

Electrochemical Testing of the Anode Materials. The electrochemical analysis was carried out at room temperature with 2032R coin-type half-cells using metallic Li foil as a counter electrode in the potential range between 0.01 and 1.5 V. The electrode was composed of *a*-SBG nanocomposites as an active material, poly(acrylic acid) (MW = 100000; Sigma-Aldrich) and sodium carboxymethyl cellulose (CMC) (MW = 90000; Sigma-Aldrich) as binder in a weight ratio of 8:1:1. The well-blended slurry was spread on copper foil, dried at 80 °C for 30 min, and then heated at 150 °C in a vacuum oven over 2 h with mass loading of 0.25−0.3 mg cm^{-2} (this loading was enough to match with the cathode material for the full cell test because of high columbic efficiency and high reversible capacity of the anode). In order to compare *a*-SBG with *c*-SiNP, another electrode was manufactured. Carbon black was present in the electrode as the conductive additive with the same loading as that of rGO in the *a*-SBG, and the other electrode conditions were the same as for the *a*-SBG electrode.

Furthermore, a natural graphite electrode was composed of 92 wt % active material and 8 wt % polyvinylidene fluoride binder. *N*-Methyl-2-pyrrolidone (NMP) was used as the solvent. After the mixed slurry was coated onto the Cu foil, the electrode was dried at 110 °C for 1 h and roll-pressed. The coin cell was manufactured in a glovebox filled with argon gas. Lithium metal foil, microporous polyethylene, and 1.3 M $LiPF_6$ in ethylene carbonate/diethyl carbonate (3:7 vol %; Panax Starlyte) with 10% fluoroethylene carbonate (Panax Starlyte, Korea) were used as the counter electrode, separator, and electrolyte, respectively. The electrochemical impedance measurement was performed using an electrochemical interface system (IVIUM). The impedance spectra were recorded by applying an AC voltage of 5 mV in amplitude in the frequency range of 0.1 Hz to 100 kHz to coin-type half-cells in a temperature bath. The obtained spectra were analyzed using ZView software. Cyclic voltammetry was performed with a CHI660D electrochemical station in the voltage range of 0.01−1.5 V (versus Li/Li^+) at various sweep rates from 0.4 to 1.0 mV s^{-1}. All electrochemical performance data were measured at room temperature in 2032 coin-type half-cells.

Electrochemical Testing of the Full Cell. The electrochemical analysis was carried out at room temperature with a 2032R coin-type full-cell using a surface-modified $LiCoO_2$ cathode as the counter electrode in the potential range between 2.5 and 4.3 V. The $LiCoO_2$ cathode electrode was mixed with active material, carbon black, and polyvinylidene fluoride binder in a weight ratio of 8:1:1. *N*-Methyl-2-pyrrolidone (NMP) was used as the solvent. After the mixed slurry was coated onto the Al foil, the electrode was dried at 110 °C for 1 h and roll-pressed. The coin cell was manufactured in a glovebox filled with argon gas. $LiCoO_2$, microporous polyethylene, and 1.3 M $LiPF_6$ in ethylene carbonate/diethyl carbonate (3:7 v/v) with 10% fluoroethylene carbonate (Panax Starlyte, Korea) were used as the counter electrode, separator, and electrolyte, respectively. The cathode and anode electrode capacities were 0.71 and 0.78 mA h cm^{-2}, respectively, with an N/P ratio (negative electrode capacity/positive electrode capacity) of 1.1. All electrochemical performance data were measured at room temperature in 2032 coin-type half-cells.

Material Characterization. To investigate the sample morphology, scanning electron microscopy (SEM, Nanonova 230, FEI) and high-resolution transmission electron microscopy (HR-TEM, JEM-2100F, JEOL) were used. The crystallinity of the samples was analyzed by X-ray diffraction (XRD, D/MAZX 2500 V/PC, Rigaku). X-ray photoelectron spectroscopy (XPS) analyses were performed with a Thermo Scientific K-Alpha spectrometer using monochromatic Al Kα radiation (1486.6 eV). Raman spectra were recorded using a 532.6 nm laser from WITec Alpha300R. The changes in the *a*-SBG and *c*-SiNP electrodes during cycling were inspected by *ex situ* SEM and TEM after the coin cells were disassembled. All electrochemical tests were performed using a WBCS-3000 (WonATech Co.).

Conflict of Interest: The authors declare no competing financial interest.

Acknowledgment. This research was supported by C-ITRC (Convergence Information Technology Research Center) support program (NIPA-2013-H0301-13-1009) supervised by the NIPA (National IT Industry Promotion Agency) through the Ministry of Science, ICT and Future Planning, Korea.

Supporting Information Available: Experimental method, *ex situ* XRD analysis of HRTEM images, electrochemical cell performance data. This material is available free of charge *via* the Internet at http://pubs.acs.org

REFERENCES AND NOTES

1. Goodenough, J. B. Evolution of Strategies for Modern Rechargeable Batteries. *Acc. Chem. Res.* **2013**, *46*, 1053–1061.
2. Thackeray, M. M.; Wolverton, C.; Isaacs, E. D. Electrical Energy Storage for Transportation—Approaching the Limits of, and Going Beyond, Lithium-Ion Batteries. *Energy Environ. Sci.* **2012**, *5*, 7854–7863.
3. Choi, N. S.; Chen, Z.; Freunberger, S. A.; Ji, X.; Sun, Y. K.; Amine, K.; Yushin, G.; Nazar, L. F.; Cho, J.; Bruce, P. G. Challenges Facing Lithium Batteries and Electrical Double-Layer Capacitors. *Angew. Chem., Int. Ed.* **2012**, *51*, 9994–10024.
4. Rolison, D. R.; Nazar, L. F. Electrochemical Energy Storage to Power the 21st Century. *MRS Bull.* **2011**, *36*, 486–493.
5. Zhang, W.-J. A Review of the Electrochemical Performance of Alloy Anodes for Lithium-Ion Batteries. *J. Power Sources* **2011**, *196*, 13–24.
6. Winter, M.; Besenhard, J. O. Electrochemical Lithiation of Tin and Tin-Based Intermetallics and Composites. *Electrochim. Acta* **1999**, *45*, 31–50.
7. Nitta, N.; Yushin, G. High-Capacity Anode Materials for Lithium-Ion Batteries: Choice of Elements and Structures

for Active Particles. *Part. Part. Syst. Char.* **2014**, *31*, 317–336.
8. Obrovac, M. N.; Christensen, L. Structural Changes in Silicon Anodes During Lithium Insertion/Extraction. *Electrochem. Solid-State Lett.* **2004**, *7*, A93–A96.
9. Hatchard, T. D.; Dahn, J. R. *In Situ* Xrd and Electrochemical Study of the Reaction of Lithium with Amorphous Silicon. *J. Electrochem. Soc.* **2004**, *151*, A838–A842.
10. Wang, J. W.; He, Y.; Fan, F.; Liu, X. H.; Xia, S.; Liu, Y.; Harris, C. T.; Li, H.; Huang, J. Y.; Mao, S. X.; et al. Two-Phase Electrochemical Lithiation in Amorphous Silicon. *Nano Lett.* **2013**, *13*, 709–715.
11. McDowell, M. T.; Lee, S. W.; Harris, J. T.; Korgel, B. A.; Wang, C.; Nix, W. D.; Cui, Y. *In Situ* Tem of Two-Phase Lithiation of Amorphous Silicon Nanospheres. *Nano Lett.* **2013**, *13*, 758–764.
12. Wu, H.; Cui, Y. Designing Nanostructured Si Anodes for High Energy Lithium Ion Batteries. *Nano Today* **2012**, *7*, 414–429.
13. Wu, H.; Chan, G.; Choi, J. W.; Ryu, I.; Yao, Y.; McDowell, M. T.; Lee, S. W.; Jackson, A.; Yang, Y.; Hu, L. B.; et al. Stable Cycling of Double-Walled Silicon Nanotube Battery Anodes through Solid-Electrolyte Interphase Control. *Nat. Nanotechnol.* **2012**, *7*, 309–314.
14. Chen, Z. H.; Christensen, L.; Dahn, J. R. Large-Volume-Change Electrodes for Li-Ion Batteries of Amorphous Alloy Particles Held by Elastomeric Tethers. *Electrochem. Commun.* **2003**, *5*, 919–923.
15. Liu, H. K.; Wang, G. X.; Guo, Z. P.; Wang, J. Z.; Konstantinov, K. The Impact of Nanomaterials on Li-Ion Rechargeable Batteries. *J. New Mater. Electrochem. Syst.* **2007**, *10*, 101–104.
16. Kim, H.; Seo, M.; Park, M. H.; Cho, J. A Critical Size of Silicon Nano-Anodes for Lithium Rechargeable Batteries. *Angew. Chem., Int. Ed.* **2010**, *49*, 2146–2149.
17. Song, J.; Chen, S.; Zhou, M.; Xu, T.; Lv, D.; Gordin, M. L.; Long, T.; Melnyk, M.; Wang, D. Micro-Sized Silicon−Carbon Composites Composed of Carbon-Coated Sub-10 Nm Si Primary Particles as High-Performance Anode Materials for Lithium-Ion Batteries. *J. Mater. Chem. A* **2014**, *2*, 1257–1262.
18. Peng, K. Q.; Wang, X.; Li, L.; Hu, Y.; Lee, S. T. Silicon Nanowires for Advanced Energy Conversion and Storage. *Nano Today* **2013**, *8*, 75–97.
19. Chan, C. K.; Peng, H.; Liu, G.; Mcllwrath, K.; Zhang, X. F.; Huggins, R. A.; Cui, Y. High-Performance Lithium Battery Anodes Using Silicon Nanowires. *Nat. Nanotechnol.* **2008**, *3*, 31–35.
20. Song, T.; Xia, J. L.; Lee, J. H.; Lee, D. H.; Kwon, M. S.; Choi, J. M.; Wu, J.; Doo, S. K.; Chang, H.; Il Park, W.; et al. Arrays of Sealed Silicon Nanotubes as Anodes for Lithium Ion Batteries. *Nano Lett.* **2010**, *10*, 1710–1716.
21. Hertzberg, B.; Alexeev, A.; Yushin, G. Deformations in Si-Li Anodes Upon Electrochemical Alloying in Nano-Confined Space. *J. Am. Chem. Soc.* **2010**, *132*, 8548–8549.
22. Park, M. H.; Kim, M. G.; Joo, J.; Kim, K.; Kim, J.; Ahn, S.; Cui, Y.; Cho, J. Silicon Nanotube Battery Anodes. *Nano Lett.* **2009**, *9*, 3844–3847.
23. Yu, Y.; Gu, L.; Zhu, C. B.; Tsukimoto, S.; van Aken, P. A.; Maier, J. Reversible Storage of Lithium in Silver-Coated Three-Dimensional Macroporous Silicon. *Adv. Mater.* **2010**, *22*, 2247–2250.
24. Kim, H.; Han, B.; Choo, J.; Cho, J. Three-Dimensional Porous Silicon Particles for Use in High-Performance Lithium Secondary Batteries. *Angew. Chem., Int. Ed.* **2008**, *47*, 10151–10154.
25. Ng, S. H.; Wang, J. Z.; Wexler, D.; Konstantinov, K.; Guo, Z. P.; Liu, H. K. Highly Reversible Lithium Storage in Spheroidal Carbon-Coated Silicon Nanocomposites as Anodes for Lithium-Ion Batteries. *Angew. Chem., Int. Ed.* **2006**, *45*, 6896–6899.
26. Magasinski, A.; Dixon, P.; Hertzberg, B.; Kvit, A.; Ayala, J.; Yushin, G. High-Performance Lithium-Ion Anodes Using a Hierarchical Bottom-up Approach. *Nat. Mater.* **2010**, *9*, 353–358.
27. Choi, S.; Lee, J.-I.; Park, S. Patterning of Electrodes for Mechanically Robust and Bendable Lithium-Ion Batteries. *J. Mater. Chem.* **2012**, *22*, 22366–22369.
28. Zhang, H.; Braun, P. V. Three-Dimensional Metal Scaffold Supported Bicontinuous Silicon Battery Anodes. *Nano Lett.* **2012**, *12*, 2778–2783.
29. Koo, B.; Kim, H.; Cho, Y.; Lee, K. T.; Choi, N. S.; Cho, J. A Highly Cross-Linked Polymeric Binder for High-Performance Silicon Negative Electrodes in Lithium Ion Batteries. *Angew. Chem., Int. Ed. Engl.* **2012**, *51*, 8762–8767.
30. Kovalenko, I.; Zdyrko, B.; Magasinski, A.; Hertzberg, B.; Milicev, Z.; Burtovyy, R.; Luzinov, I.; Yushin, G. A Major Constituent of Brown Algae for Use in High-Capacity Li-Ion Batteries. *Science* **2011**, *334*, 75–79.
31. Wang, C.; Wu, H.; Chen, Z.; McDowell, M. T.; Cui, Y.; Bao, Z. Self-Healing Chemistry Enables the Stable Operation of Silicon Microparticle Anodes for High-Energy Lithium-Ion Batteries. *Nat. Chem.* **2013**, *5*, 1042–1048.
32. Liu, N.; Wu, H.; McDowell, M. T.; Yao, Y.; Wang, C. M.; Cui, Y. A Yolk-Shell Design for Stabilized and Scalable Li-Ion Battery Alloy Anodes. *Nano Lett.* **2012**, *12*, 3315–3321.
33. Moon, T.; Kim, C.; Park, B. Electrochemical Performance of Amorphous-Silicon Thin Films for Lithium Rechargeable Batteries. *J. Power Sources* **2006**, *155*, 391–394.
34. Shin, H. C.; Corno, J. A.; Gole, J. L.; Liu, M. L. Porous Silicon Negative Electrodes for Rechargeable Lithium Batteries. *J. Power Sources* **2005**, *139*, 314–320.
35. He, Y.; Yu, X. Q.; Wang, Y. H.; Li, H.; Huang, X. J. Alumina-Coated Patterned Amorphous Silicon as the Anode for a Lithium-Ion Battery with High Coulombic Efficiency. *Adv. Mater.* **2011**, *23*, 4938–4941.
36. Baggetto, L.; Danilov, D.; Notten, P. H. Honeycomb-Structured Silicon: Remarkable Morphological Changes Induced by Electrochemical (De)Lithiation. *Adv. Mater.* **2011**, *23*, 1563–1566.
37. Pal, S.; Damle, S. S.; Patel, S. H.; Datta, M. K.; Kumta, P. N.; Maiti, S. Modeling the Delamination of Amorphous-Silicon Thin Film Anode for Lithium-Ion Battery. *J. Power Sources* **2014**, *246*, 149–159.
38. McDowell, M. T.; Lee, S. W.; Nix, W. D.; Cui, Y. 25th Anniversary Article: Understanding the Lithiation of Silicon and Other Alloying Anodes for Lithium-Ion Batteries. *Adv. Mater.* **2013**, *25*, 4966–4985.
39. Fedorov, A. S.; Popov, Z. I.; Kuzubov, A. A.; Ovchinnikov, S. G. Theoretical Study of the Diffusion of Lithium in Crystalline and Amorphous Silicon. *JETP Lett.* **2012**, *95*, 143–147.
40. Lee, J. K.; Smith, K. B.; Hayner, C. M.; Kung, H. H. Silicon Nanoparticles-Graphene Paper Composites for Li Ion Battery Anodes. *Chem. Commun.* **2010**, *46*, 2025–2027.
41. Nguyen, B. P. N.; Kumar, N. A.; Gaubicher, J.; Duclairoir, F.; Brousse, T.; Crosnier, O.; Dubois, L.; Bidan, G.; Guyomard, D.; Lestriez, B. Nanosilicon-Based Thick Negative Composite Electrodes for Lithium Batteries with Graphene as Conductive Additive. *Adv. Energy Mater.* **2013**, *3*, 1351–1357.
42. Yang, S. B.; Feng, X. L.; Ivanovici, S.; Mullen, K. Fabrication of Graphene-Encapsulated Oxide Nanoparticles: Towards High-Performance Anode Materials for Lithium Storage. *Angew. Chem., Int. Ed.* **2010**, *49*, 8408–8411.
43. Jiang, X.; Yang, X.; Zhu, Y.; Shen, J.; Fan, K.; Li, C. *In Situ* Assembly of Graphene Sheets-Supported Sns2 Nanoplates into 3d Macroporous Aerogels for High-Performance Lithium Ion Batteries. *J. Power Sources* **2013**, *237*, 178–186.
44. Evanoff, K.; Magasinski, A.; Yang, J. B.; Yushin, G. Nanosilicon-Coated Graphene Granules as Anodes for Li-Ion Batteries. *Adv. Energy Mater.* **2011**, *1*, 495–498.
45. Ji, L.; Zheng, H.; Ismach, A.; Tan, Z.; Xun, S.; Lin, E.; Battaglia, V.; Srinivasan, V.; Zhang, Y. Graphene/Si Multilayer Structure Anodes for Advanced Half and Full Lithium-Ion Cells. *Nano Energy* **2012**, *1*, 164–171.
46. Liang, M. H.; Zhi, L. J. Graphene-Based Electrode Materials for Rechargeable Lithium Batteries. *J. Mater. Chem.* **2009**, *19*, 5871–5878.
47. Zhou, X.; Yin, Y. X.; Wan, L. J.; Guo, Y. G. Facile Synthesis of Silicon Nanoparticles Inserted into Graphene Sheets as

Improved Anode Materials for Lithium-Ion Batteries. *Chem. Commun.* **2012**, *48*, 2198–2200.
48. Zhou, X.; Yin, Y.-X.; Wan, L.-J.; Guo, Y.-G. Self-Assembled Nanocomposite of Silicon Nanoparticles Encapsulated in Graphene through Electrostatic Attraction for Lithium-Ion Batteries. *Adv. Energy Mater.* **2012**, *2*, 1086–1090.
49. Zhao, X.; Hayner, C. M.; Kung, M. C.; Kung, H. H. In-Plane Vacancy-Enabled High-Power Si-Graphene Composite Electrode for Lithium-Ion Batteries. *Adv. Energy Mater.* **2011**, *1*, 1079–1084.
50. Jung, D. S.; Hwang, T. H.; Park, S. B.; Choi, J. W. Spray Drying Method for Large-Scale and High-Performance Silicon Negative Electrodes in Li-Ion Batteries. *Nano Lett.* **2013**, *13*, 2092–2097.
51. Li, H.; Huang, X. J.; Chen, L. Q.; Wu, Z. G.; Liang, Y. A High Capacity Nano-Si Composite Anode Material for Lithium Rechargeable Batteries. *Electrochem. Solid-State Lett.* **1999**, *2*, 547–549.
52. Liu, N.; Lu, Z. D.; Zhao, J.; McDowell, M. T.; Lee, H. W.; Zhao, W. T.; Cui, Y. A Pomegranate-Inspired Nanoscale Design for Large-Volume-Change Lithium Battery Anodes. *Nat. Nanotechnol.* **2014**, *9*, 187–192.
53. Chang, J.; Huang, X.; Zhou, G.; Cui, S.; Hallac, P. B.; Jiang, J.; Hurley, P. T.; Chen, J. Multilayered Si Nanoparticle/Reduced Graphene Oxide Hybrid as a High-Performance Lithium-Ion Battery Anode. *Adv. Mater.* **2014**, *26*, 758–764.
54. Liu, X. H.; Zhong, L.; Huang, S.; Mao, S. X.; Zhu, T.; Huang, J. Y. Size-Dependent Fracture of Silicon Nanoparticles During Lithiation. *ACS Nano* **2012**, *6*, 1522–1531.
55. Hummers, W. S.; Offeman, R. E. Preparation of Graphitic Oxide. *J. Am. Chem. Soc.* **1958**, *80*, 1339–1339.